Coherent Control of GHz Resonant Modes by an Integrated Acoustic Etalon

Huarui Sun,[1] Vladimir A. Stoica,[2,5] Max Shtein,[3,5] Roy Clarke,[2,5] and Kevin P. Pipe[1,4,5,*]

[1]*Department of Mechanical Engineering, University of Michigan, Ann Arbor, Michigan 48109-2125, USA*
[2]*Department of Physics, University of Michigan, Ann Arbor, Michigan 48109-1040, USA*
[3]*Department of Materials Science and Engineering, University of Michigan, Ann Arbor, Michigan 48109-2136, USA*
[4]*Department of Electrical Engineering and Computer Science, University of Michigan, Ann Arbor, Michigan 48109-2122, USA*
[5]*Center for Solar and Thermal Energy Conversion (CSTEC), University of Michigan, Ann Arbor, Michigan 48109, USA*

By carefully tuning the thickness of a compliant thin film placed within an acoustic cavity, we achieve coherent control of the cavity's acoustic resonances, analogous to the operation of an optical etalon. This technique is demonstrated using a supported membrane oscillator in which multiple high-frequency harmonic resonances are simultaneously optoexcited by an ultrafast laser. Theoretical and computational methods are used to analyze the selective strengthening or suppression of these resonances by constructive or destructive interference.

Optoexcited micromechanical resonators have recently attracted a great deal of attention due to interesting behavior associated with the coupling of light with high frequency acoustic vibrational modes [1–4]. Optical actuation affords numerous possibilities for active (excitation-based) coherent control of vibrational dynamics [5,6]; for example, timing of optical driving pulses [7] and tuning of optical field strength [1] have each been demonstrated as a means to selectively strengthen or suppress multiple resonances within a given acoustic spectrum. Passive techniques based on free-space optical cavities [8] or structure modification can likewise provide coherent control; for example, optical [9] and acoustic [10] distributed Bragg reflectors integrated within a resonator structure have each been shown to increase the amplitude of a transduced acoustic mode.

The absorption of a femtosecond optical pulse by a material typically results in impulsive strain that is broadband with a spectral width greater than 100 GHz [11]. In free-standing membrane structures recently considered for high-frequency (10 + GHz) acoustic resonator applications, this spectral width is large enough to simultaneously excite the membrane's resonant longitudinal acoustic modes up to the 15th harmonic (285 GHz) [12,13].

Coherent control techniques to select a certain mode from a relatively broadband comb of excited cavity modes are relatively common in optics. In solid state lasers, optical etalons are used to achieve tunable single longitudinal mode output by suppressing modes that are adjacent to a selected wavelength [14,15]. Here we propose and demonstrate an integrated acoustic etalon as a passive means for the selective strengthening or suppression of multiple resonances within an acoustic cavity.

We consider a supported rather than free-standing membrane resonator, the former being more practical in its ability to directly couple acoustic modes to external media. The acoustic dynamics of supported thin films under ultrafast laser excitation have been the subject of several recent studies [8,16–20]. The absorption of laser pulses by a metal transducer in contact with a relatively hard material such as silicon or sapphire is known to lead to a train of acoustic echoes (rather than excited vibrational modes of the film) if the metal thickness is much larger than the optical penetration depth [8,16]. If the transducer thickness is reduced to the order of the optical penetration depth, direct coupling of energy from the laser pulse to the first resonant vibrational mode of the transducer leads to strong excitation of this mode. Because of the small film thickness in this case, however, higher-order modes are typically above the spectral range of the transduced acoustic pulse and therefore either absent or only very weakly excited [17,21,22].

As shown below, a compliant organic supporting film can allow multiple vibrational modes to be strongly optoexcited in a relatively thick metallic resonator, and furthermore can be employed as the acoustic equivalent of an optical etalon to control the resulting mode spectrum within the acoustic cavity. Similar to the optical analog, this mode control is accomplished by placing the etalon within the cavity and utilizing its Fabry-Perot transmission maxima (at which wavelengths the cavity field is concentrated within the etalon [15]) or its reflection maxima (where the etalon acts as a resonant reflector [15]) to retain or reject desired cavity modes. For the specific acoustic etalon described here, several transmission and reflection maxima fall within the bandwidth of excited acoustic modes; the etalon therefore acts as a resonant transmitter for certain modes and a resonant reflector for other modes; it can therefore be used to select a certain resonant mode, tune the resonant mode frequencies, or introduce additional resonances into the system.

The resonant vibrational modes of a thin film occur at frequency spacings of $v/2d$, where v is the acoustic velocity and d is the film thickness, while the peak frequency of the initial strain wave caused by laser pulse absorption is

$v/2\pi\zeta$, where ζ is the optical penetration depth (approximately 8 nm in aluminum for $\lambda = 1560$ nm light) [11]. To significantly excite a range of resonator modes (here we choose modes up to the 4th harmonic) therefore requires $d > 4\pi\zeta \approx 100$ nm. Because hot electron diffusion can increase the region of thermal stress beyond the optical penetration depth [11,23], we choose a conservative resonator thickness of 200 nm. An aluminum film of this thickness and a film of copper phthalocyanine (CuPc) are both deposited using vacuum thermal evaporation on a [100] silicon substrate (Fig. 1). The compliant CuPc film is sandwiched between the Al and Si, allowing the Al membrane to vibrate in its fundamental and harmonic modes and acting as a Fabry-Perot etalon for the acoustic waves which are confined in the cavity formed by the strong acoustic impedance mismatches at the Al/air and CuPc/Si interfaces. To demonstrate the spectral control afforded by the CuPc etalon, a series of samples is made in which the etalon thickness is varied from 0 to 77 nm. The resonator is then excited and its acoustic properties characterized using an ultrafast pump-probe setup in an asynchronous optical sampling (ASOPS) configuration [24], which provides a high signal-to-noise ratio ($> 10^7$) and a high dynamic range (fs-to-ns), thereby allowing measurement of GHz coherent acoustic resonances over long times (see Supplemental Material [25] for further details).

For small values of the CuPc thickness ($d_{\mathrm{CuPc}} < 7$ nm), the Al membrane is insufficiently decoupled from the Si substrate for resonant membrane modes to be excited, and the resulting time dynamics (Fig. 1) exhibit a series of echoes that grow in intensity as the CuPc thickness increases due to increasing acoustic impedance contrast. For CuPc thicknesses of 7 nm and greater, the excitation of resonant membrane modes is clearly visible; Fourier transforms reveal the simultaneous excitation of up to five resonant modes. This transition in acoustic dynamics from

an echo regime to a resonant vibration regime is enabled by two effects. First, a greater CuPc thickness represents a larger effective acoustic impedance mismatch and hence increased acoustic confinement within the Al film. Second, the stiffnesses of soft organic thin films have been shown to scale inversely with the film thickness [26–28].

Supported films, when acoustically decoupled from their surroundings, have quantized longitudinal acoustic modes at $f_n = nv/4d$. Whether the resonator exhibits odd-order or even-order modes is determined by the ratio of the acoustic impedances (Z_f/Z_s) of the film and its supporting material [18,29]: n is odd when $Z_f/Z_s < 1$ and even when $Z_f/Z_s > 1$.

The resonant frequencies of an Al/CuPc bilayer on a Si substrate obey the following equation [21]:

$$r_{\mathrm{Al/CuPc}} \exp\left(-2j\omega_m \frac{d_{\mathrm{Al}}}{v_{\mathrm{Al}}}\right)$$
$$+ r_{\mathrm{CuPc/Si}} \exp\left[-2j\omega_m \left(\frac{d_{\mathrm{Al}}}{v_{\mathrm{Al}}} + \frac{d_{\mathrm{CuPc}}}{v_{\mathrm{CuPc}}}\right)\right]$$
$$- r_{\mathrm{Al/CuPc}} r_{\mathrm{CuPc/Si}} \exp\left(-2j\omega_m \frac{d_{\mathrm{CuPc}}}{v_{\mathrm{CuPc}}}\right) - 1 = 0, \quad (1)$$

where ω_m is the quantized angular frequency of the mth resonant mode, $r_{\mathrm{Al/CuPc}}$ and $r_{\mathrm{CuPc/Si}}$ are the acoustic reflection coefficients at the respective interfaces, and d_{CuPc} and d_{Al} are the thicknesses of the respective films. By definition, $r_{\mathrm{Al/CuPc}} = (\rho_{\mathrm{Al}}v_{\mathrm{Al}} - \rho_{\mathrm{CuPc}}v_{\mathrm{CuPc}})/(\rho_{\mathrm{Al}}v_{\mathrm{Al}} + \rho_{\mathrm{CuPc}}v_{\mathrm{CuPc}})$ and $r_{\mathrm{CuPc/Si}} = (\rho_{\mathrm{CuPc}}v_{\mathrm{CuPc}} - \rho_{\mathrm{Si}}v_{\mathrm{Si}})/(\rho_{\mathrm{CuPc}}v_{\mathrm{CuPc}} + \rho_{\mathrm{Si}}v_{\mathrm{Si}})$, where the assumed densities and sound velocities are $\rho_{\mathrm{Al}} = 2700$ kg/m^3, $\rho_{\mathrm{CuPc}} = 1600$ kg/m^3, and $v_{\mathrm{Al}} = 6420$ m/s. While no literature data are available for the speed of sound in CuPc, well-calibrated measurements of organic materials such as PMMA [poly(methyl methacrylate)] report values in the range of 2500–3000 m/s [30]. We allow v_{CuPc} to be the only fitting parameter in what follows, deriving a value of $3000 +/- 200$ m/s. Resonant frequencies measured for the samples are plotted as blue circles in Fig. 2 inset, while resonant frequencies calculated from Eq. (1) are plotted as red lines. At zero CuPc thickness, the resonant frequencies correspond to the odd order modes of the 200 nm Al film, as expected for the Al/Si structure ($Z_{\mathrm{Al}}/Z_{\mathrm{Si}} < 1$). The addition of the CuPc layer ($Z_{\mathrm{Al}}/Z_{\mathrm{CuPc}} > 1$) shifts the resonant frequencies toward the even-order modes of the Al film (f_{Al}, dashed lines).

For certain CuPc thicknesses (at which the solid red and dashed black lines cross), the Al/CuPc bilayer resonant modes line up with f_{Al}. At these thicknesses, the CuPc layer acts as a $\lambda/4$ resonant reflector, greatly increasing the measured mode amplitude as shown in Fig. 2. Similar to an optical etalon in a laser cavity, the CuPc film thereby selects one (or more) of the relatively broadband comb of resonant modes excited by the laser pulse. As shown in Fig. 1, 18 and 50 nm thick CuPc films select the 2nd and 1st mode, respectively; the selected mode then dominates the ringing of the resonator after the first ~250 ps.
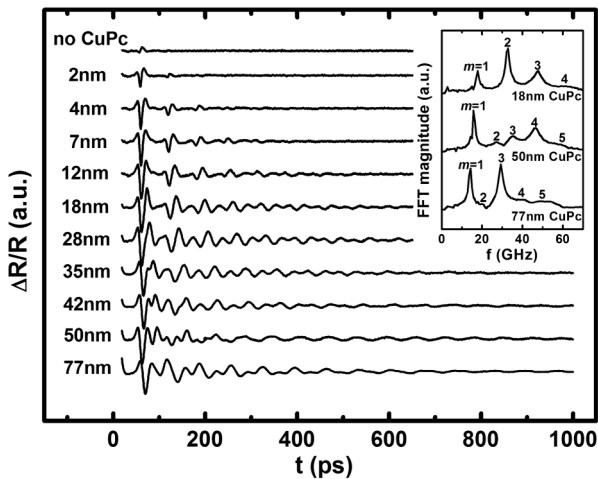

FIG. 1. Acoustic transients of optically excited Al/CuPc films on Si with varied CuPc thickness. Inset: Fourier spectra of acoustic transients for samples with 18, 50, and 77 nm thick CuPc layers.
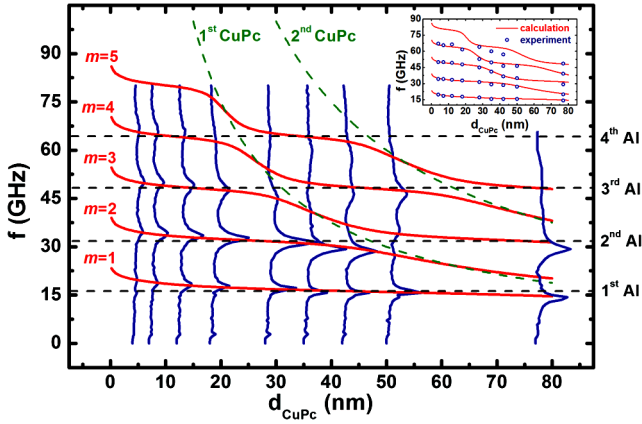
FIG. 2 (color online).   Resonant frequencies of Al/CuPc films calculated from Eq. (1) (red lines) and Fourier spectra of acoustic transients. Dashed lines represent the natural frequencies of a free-standing 200 nm thick Al film and a free-standing CuPc film. Inset shows measured resonant frequencies as blue circles (all points having an error of $+/-0.7$ GHz).

The acoustic reflectivity of a CuPc film sandwiched between an Al film and a Si substrate can be calculated through a transfer matrix approach:

$$R_{\text{Al/CuPc/Si}}$$

$$= \frac{(r_{\text{Al/CuPc}} + r_{\text{CuPc/Si}})^2 - 4r_{\text{Al/CuPc}}r_{\text{CuPc/Si}}\sin^2\left(\frac{\pi}{2}\frac{d_{\text{CuPc}}}{\lambda_{\text{CuPc}}}\right)}{(1 + r_{\text{Al/CuPc}}r_{\text{CuPc/Si}})^2 - 4r_{\text{Al/CuPc}}r_{\text{CuPc/Si}}\sin^2\left(\frac{\pi}{2}\frac{d_{\text{CuPc}}}{\lambda_{\text{CuPc}}}\right)},$$
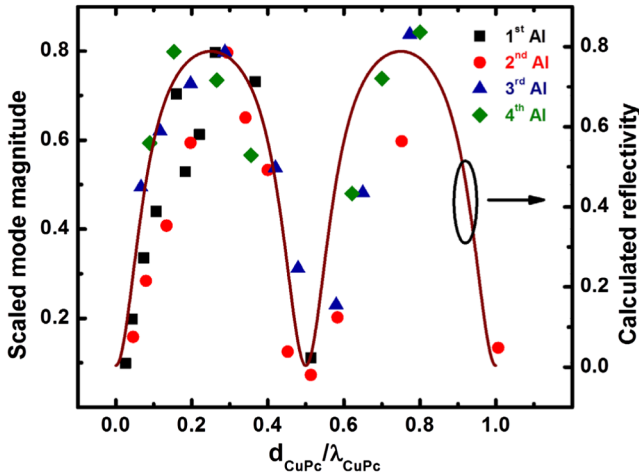
(2)

FIG. 3 (color online).   Measured magnitudes for modes near the corresponding free-standing Al film resonance as a function of CuPc film thickness (scaled by the mode wavelength in CuPc), demonstrating the nature of the CuPc film as a resonant reflector. Also shown is the CuPc film acoustic reflectivity calculated using Eq. (2). Because the initial energy in each mode (which could provide a baseline for all modes) is not certain, each series (1st Al, 2nd Al, etc.) is scaled by its maximum magnitude.

where λ_{CuPc} is the acoustic wavelength in CuPc. Figure 3 compares the measured magnitude of each mode to the calculated CuPc layer reflectivity, demonstrating that the layer acts to selectively contain certain modes within the cavity through acoustic interference (e.g., CuPc layers corresponding to $d_{\text{CuPc}}/\lambda_{\text{CuPc}}$ of 0.25 and 0.5 represent quarter-wavelength and half-wavelength coatings). The fact that the mode amplitudes are observed to increase with increasing CuPc thickness suggests that surface and attenuation effects are small compared to the effect of coherent reflection at the cavity walls.

We employ a finite-difference time-domain method to compute the displacement field of each resonant mode within the Al/CuPc bilayer. In this technique, we oscillate the position of the Al/air interface at a certain frequency with constant stress amplitude (1 MPa, which is realistic for laser-excited stress in Al) and calculate the corresponding standing wave at this frequency that remains when all transients have decayed to zero. Figure 4 plots the standing wave displacement profiles in the frequency range of 10–55 GHz for several cavities with different CuPc thicknesses. Resonant modes can be identified by the frequencies for which the standing wave amplitude is locally maximized; the resonant frequencies identified by this finite-difference time-domain method are identical to those calculated using Eq. (1). The contour plots show that acoustic modes occur near the even order natural frequencies of Al (16, 32, and 48 GHz, etc.) in samples with CuPc and near the odd order natural frequencies of Al (24, 40 GHz, etc.) in samples without CuPc (where the low impedance mismatch between Al and Si reduces the mode strength). The former resonances appear in Fig. 1 as 17.9, 32.9, 47.9, and 61.7 GHz ($m = 1, 2, 3, 4$) in the 18 nm CuPc sample, 15.7, 35.0, 46.4, and 58.9 GHz ($m = 1, 3, 4, 5$) in the 50 nm CuPc sample, and 14.3, 29.3, and 48.6 GHz
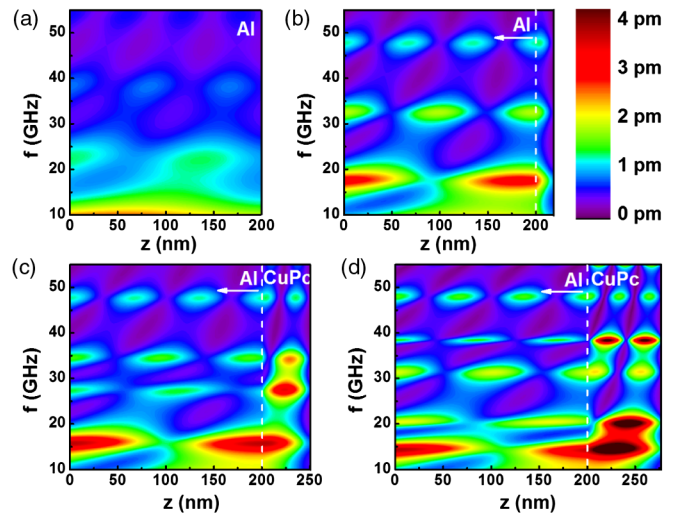

FIG. 4 (color online).   Calculated displacement contours for (a) no CuPc layer, (b) 18 nm CuPc layer, (c) 50 nm CuPc layer, and (d) 77 nm CuPc layer.

($m = 1, 3, 5$) in the 77 nm CuPc sample, all values $+/-$ 0.7 GHz. For these resonances, the acoustic energy is rather evenly distributed in the Al and CuPc films, and the CuPc layer selects modes of the Al transducer by promoting constructive or destructive interference.

In Figs. 4(c) and 4(d), additional modes are predicted between adjacent Al resonances (28 GHz for 50 nm CuPc, and 20 and 39 GHz for 77 nm CuPc). These frequencies correspond to the Fabry-Perot resonances of the CuPc layer itself, for which acoustic intensity in the cavity is primarily confined within the CuPc etalon rather than in Al. The presence of these additional modes is confirmed in Fig. 1, where a peak at 27.1 GHz ($m = 2$) is apparent in the 50 nm CuPc sample and two small peaks at 20.0 GHz ($m = 2$) and 39.2 GHz ($m = 4$) are weakly visible in the 77 nm CuPc sample. Like its optical analog, the acoustic etalon selects the modes at its Fabry-Perot resonances, acting as a band pass filter for acoustic waves near these frequencies and thereby allowing a standing wave at these frequencies to develop in the cavity defined by the air/Al and CuPc/Si
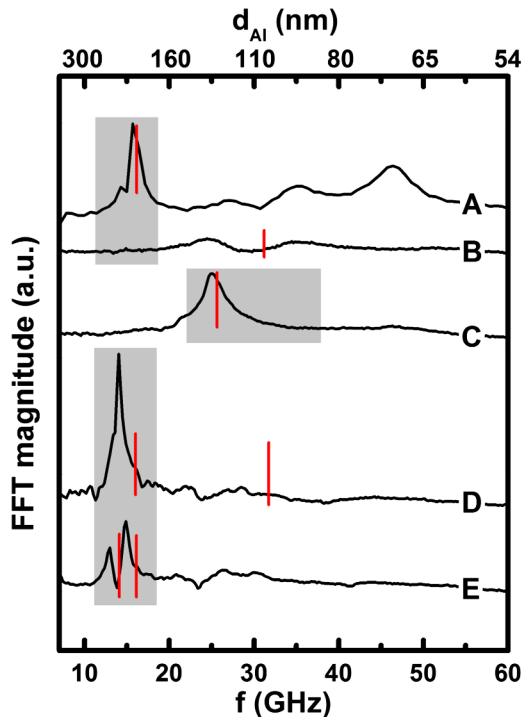

FIG. 5 (color online). Fourier spectra of acoustic transients for Samples *A-E* with the following layer structures from top to bottom deposited on Si substrates: *A*, 200 nm Al/50 nm CuPc; *B*, 103 nm Al/50 nm CuPc; *C*, 125 nm Al/25 nm CuPc; *D*, 200 nm Al/50 nm CuPc/103 nm Al/50 nm CuPc; *E*, 200 nm Al/ 50 nm CuPc/222 nm Al/50 nm CuPc. The bottom *x* axis shows the fundamental resonant frequency for a free-standing Al film of the thickness given on the top *x* axis. The short red lines indicate the measured Al thicknesses in each sample. The shaded regions indicate the reflection band of the CuPc etalon(s) in each sample (defined as the frequency range for which the etalon's acoustic reflectivity is greater than 0.75).

interfaces. In this way the etalon introduces its own resonances into the spectrum of the membrane resonator.

Further illustrations of the use of acoustic etalons to control resonant acoustic spectra are given in Fig. 5. Sample *A* is the 50 nm CuPc sample shown in Fig. 1. Sample *B* uses a thin Al resonator, causing the fundamental resonance to be shifted to 31.2 GHz, where the 50 nm etalon is not reflective; the mode therefore leaks out of the cavity and does not appear in the spectrum. Sample *C* uses both a thin Al layer and a thin etalon; since the fundamental resonance is now within the reflection band of the etalon, the peak again appears. Sample *D* uses a thick Al film, a thin Al film, and two thick etalons. The fundamental resonance of the thin Al film is outside the reflection band of the two etalons (as in Sample *B*), so it does not appear; however, the thin Al film is half as thick as the thick Al film and thus acts as a resonant reflector. The resonance of the thick Al film is therefore strengthened relative to Sample *A*, as it sits on three quarter-wave reflectors. Sample *E* uses two thick Al films of slightly different thickness and two thick etalons. Because the etalons act as resonant reflectors for the fundamental modes of both Al films, the two resonators are both activated, with two peaks appearing in the spectrum that correspond to their resonances. The spectrum of a coupled oscillator system is controlled in this sample; while the measurement only probes the top resonator, the modes of both the top and bottom resonators are present. While a model significantly more sophisticated than Eq. (1) will be necessary to provide complete analysis of such dual-resonator samples, we believe it to be intuitive that mass loading by the relatively heavy second Al layer is the primary cause of the larger red shifts observed in Samples *D* and *E* relative to the natural (unloaded) Al film resonances.

In conclusion, we have shown how a compliant supporting layer can allow multiple harmonics to persist simultaneously in a supported membrane resonator, the dynamics of which differ fundamentally from the echo behavior typically observed when metal transducers are placed on noncompliant substrates [8,16,19]. Because the compliant layer forms part of the acoustic cavity, various compliant layer thicknesses can be used to generate constructive or destructive interference of the membrane's resonant modes, thereby allowing coherent control and mode selection analogous to an optical etalon. Furthermore, the acoustic etalon can provide strong confinement for acoustic energy at its own resonances, and can add these resonances to the system. By including multiple resonators and etalons within a layer stack, significant control over the system's acoustic dynamics can be achieved, supporting future studies of coupled high-frequency acoustic oscillators, stimulated emission of phonons, acoustic mode switching, and the mechanical properties of thin films.

------

*Corresponding author.
pipe@umich.edu

[1] T. Carmon and K. J. Vahala, Phys. Rev. Lett. **98**, 123901 (2007).

[2] S. Gröblacher, K. Hammerer, M. R. Vanner, and M. Aspelmeyer, Nature (London) **460**, 724 (2009).

[3] V. Juvé, A. Crut, P. Maioli, M. Pellarin, M. Broyer, N. Del Fatti, and F. Vallée, Nano Lett. **10**, 1853 (2010).

[4] T. A. Kelf, Y. Tanaka, O. Matsuda, E. M. Larsson, D. S. Sutherland, and O. B. Wright, Nano Lett. **11**, 3893 (2011).

[5] D. H. Hurley, R. Lewis, O. B. Wright, and O. Matsuda, Appl. Phys. Lett. **93**, 113101 (2008).

[6] C.-K. Sun, Y.-K. Huang, J.-C. Liang, A. Abare, and S. P. DenBaars, Appl. Phys. Lett. **78**, 1201 (2001).

[7] G. S. Wiederhecker, A. Brenn, H. L. Fragnito, and P. St. J. Russell, Phys. Rev. Lett. **100**, 203903 (2008).

[8] Y. Li, Q. Miao, A. V. Nurmikko, and H. J. Maris, J. Appl. Phys. **105**, 083516 (2009).

[9] N. D. Lanzillotti-Kimura, A. Fainstein, A. Huynh, B. Perrin, B. Jusserand, A. Miard, and A. Lemaître, Phys. Rev. Lett. **99**, 217405 (2007).

[10] N. D. Lanzillotti-Kimura, A. Fainstein, B. Perrin, B. Jusserand, A. Soukiassian, X. X. Xi, and D. G. Schlom, Phys. Rev. Lett. **104**, 187402 (2010).

[11] O. B. Wright and V. E. Gusev, IEEE Trans. Ultrason. Ferroelectr. Freq. Control **42**, 331 (1995).

[12] F. Hudert, A. Bruchhausen, D. Issenmann, O. Schecker, R. Waitz, A. Erbe, E. Scheer, T. Dekorsy, A. Mlayah, and J.-R. Huntzinger, Phys. Rev. B **79**, 201307(R) (2009).

[13] A. Bruchhausen, R. Gebs, F. Hudert, D. Issenmann, G. Klatt, A. Bartels, O. Schecker, R. Waitz, A. Erbe, E. Scheer, J.-R. Huntzinger, A. Mlayah, and T. Dekorsy, Phys. Rev. Lett. **106**, 077401 (2011).

[14] P. W. Smith, Proc. IEEE **60**, 422 (1972).

[15] W. Koechner, *Solid-State Laser Engineering* (Springer, New York, 2006), 6th ed.

[16] G. A. Antonelli, B. Perrin, B. C. Daly, and D. G. Cahill, Mater. Res. Soc. Bull. **31**, 607 (2006).

[17] M. Hettich, A. Bruchhausen, S. Riedel, T. Geldhauser, S. Verleger, D. Issenmann, O. Ristow, R. Chauhan, J. Dual, A. Erbe, E. Scheer, P. Leiderer, and T. Dekorsy, Appl. Phys. Lett. **98**, 261908 (2011).

[18] A. V. Akimov, E. S. K. Young, J. S. Sharp, V. Gusev, and A. J. Kent, Appl. Phys. Lett. **99**, 021912 (2011).

[19] B. C. Daly, K. Kang, Y. Wang, and D. G. Cahill, Phys. Rev. B **80**, 174112 (2009).

[20] C. Mechri, P. Ruello, and V. Gusev, New J. Phys. **14**, 023048 (2012).

[21] B. Bonello, G. Louis, and P. Battioni, Rev. Sci. Instrum. **74**, 889 (2003).

[22] H. Ogi, M. Fujii, N. Nakamura, T. Yasui, and M. Hirao, Phys. Rev. Lett. **98**, 195503 (2007).

[23] G. Tas and H. J. Maris, Phys. Rev. B **49**, 15 046 (1994).

[24] V. A. Stoica, Y.-M. Sheu, D. A. Reis, and R. Clarke, Opt. Express **16**, 2322 (2008).

[25] See Supplemental Material at http://link.aps.org/supplemental/10.1103/PhysRevLett.110.086109 for further details of the ultrafast optical pump-probe measurement.

[26] G. Tas, J. J. Loomis, H. J. Maris, A. A. Bailes, and L. E. Seiberling, Appl. Phys. Lett. **72**, 2235 (1998).

[27] J. M. Torres, N. Bakken, C. M. Stafford, J. Li, and B. D. Vogt, Soft Matter **6**, 5783 (2010).

[28] P. A. O'Connell and G. B. McKenna, Eur. Phys. J. E **20**, 143 (2006).

[29] J. Groenen, F. Poinsotte, A. Zwick, C. M. Sotomayor Torres, M. Prunnila, and J. Ahopelto, Phys. Rev. B **77**, 045420 (2008).

[30] C. J. Morath and H. J. Maris, Phys. Rev. B **54**, 203 (1996).